IEEE Access
Multidisciplinary | Rapid Review | Open Access Journal

Received February 8, 2022, accepted April 11, 2022, date of publication April 14, 2022, date of current version April 26, 2022.

*Digital Object Identifier 10.1109/ACCESS.2022.3167422*

# Customized Radiofrequency Phased-Array Coil Combining Transmit-Only, Receive-Only, and Transmit/Receive Coils for Magnetic Resonance Imaging of Visual Cortex at 7 Tesla

**HYEONG-SEOP KIM[1,2], BYUNG-PAN SONG[1,2], ROYOUNG KIM[2,3], WOO-CHUL CHOI[4], DONGHYUK KIM[5], WON MOK SHIM[1,2,3], KYOUNG-NAM KIM[6], AND SEUNG-KYUN LEE[1,2,3,7]**

[1]Department of Intelligent Precision Healthcare Convergence, Sungkyunkwan University, Suwon 16419, Republic of Korea
[2]Center for Neuroscience Imaging Research, Institute for Basic Science, Sungkyunkwan University, Suwon 16419, Republic of Korea
[3]Department of Biomedical Engineering, Sungkyunkwan University, Suwon 16419, Republic of Korea
[4]Department of Bio and Brain Engineering, Korea Advanced Institute of Science and Technology, Daejeon 34141, Republic of Korea
[5]GAIHST, Department of Health Sciences and Technology, Gachon University, Incheon 21999, Republic of Korea
[6]Department of Biomedical Engineering, Gachon University, Incheon 21936, Republic of Korea
[7]Department of Physics, Sungkyunkwan University, Suwon 16419, Republic of Korea

Corresponding authors: Kyoung-Nam Kim (kyoungnam.kim@gachon.ac.kr) and Seung-Kyun Lee (lee.seungkyun@gmail.com)

This work was supported in part by the Institute for Basic Science under Grant IBS-R015-D1, and in part by the Institute for Information & Communications Technology Promotion (IITP) funded by the Korean Government (MSIP) through the Development of Precision Analysis and Imaging Technology for Biological Radio Waves under Grant 2021-0-00490.

**ABSTRACT** Magnetic resonance imaging (MRI) using an ultra-high magnetic field (7 Tesla) enables detailed and non-invasive studies of the function and anatomy of the human visual cortex, which is the brain region responsible for visual signal processing. However, 7T human MRI often suffers from image shading in the occipital region due to the radiofrequency (RF) wave propagation effect. Dedicated visual cortex coils, on the other hand, often lack the capability to visualize the whole brain which is necessary for image registration. We propose a novel RF coil structure in which a 2-channel transmit and receive (TRx) coil is grafted onto the frontal part of a multi-channel transmit-only/receive-only (TORO, 4Tx/14Rx) visual cortex coil. This coil was tested for high-resolution functional MRI with an in-plane resolution of 0.5 mm. The results showed that the proposed coil achieved a higher ($\times$2.5) temporal signal-to-noise ratio (tSNR) in functional imaging of the visual cortex area than that of a commercial 7T whole-head coil. The added 2-channel TRx elements allowed whole-brain edge images to be acquired, enabling successful brain segmentation and atlas registration without the need for a second scan using a whole-head coil. The proposed coil structure can be useful for high-resolution visual functional MRI at very high magnetic fields due to its sensitivity, open geometry, and compatibility with the standard image processing workflow.

**INDEX TERMS** Visual cortex, RF coil, TORO coil, combined TRx coil, magnetic resonance imaging, functional MRI.

## I. INTRODUCTION

In recent years, human magnetic resonance imaging (MRI) systems operating at a static magnetic field of 7 Tesla (7T) have been available for clinical diagnostics and basic research, paving the way for widespread application of ultra-high-field MRI for improved visualization and imaging of the human brain. 7T MRI allows fine, mesoscale structures in the retinotopic visual regions to be visualized and detected, as increased sensitivity enables imaging of the visual cortex

The associate editor coordinating the review of this manuscript and approving it for publication was Jinhua Sheng.

with smaller voxels. For example, 7T MRI was reported to have a signal-to-noise ratio (SNR) that is 70% higher than 3T MRI at a resolution of 1.1 $mm^3$ [1] and a contrast-to-noise ratio (CNR) that is approximately twice that of 3T MRI [2]. However, imaging at such high magnetic fields (above 3T) presents several challenges such as radiofrequency (RF) wave propagation effect in biological tissues that causes image shading and contrast variation [3]–[5]. Therefore, RF shimming and parallel transmission (pTx) [6], [7] based on RF transmit field (B1+) mapping [8], [9] have been developed to address this problem. The transmit (Tx) efficiency of a circularly polarized (CP) birdcage coil in the ultra-high magnetic fields tends to peak near the center of the head, resulting in image shading around the occipital region of the brain, including the visual cortex [10]. Therefore, a phased array transmit coil has been widely used [10]–[12] for brain cortical imaging in 7T MRI. The Tx efficiency can be maximized in the visual cortex by optimizing the phase of the transmit array [13]. In addition, the phased array transmit coils can alleviate the specific absorption rate (SAR) problem in high fields and improve the general image quality through more homogeneous spin excitation [14].

Regarding receive (Rx) coils, it is known that multi-element receiver coils can improve the SNR [15]–[19] because the body noise decreases as the loop size decreases, while the spin signal from regions close to the loop increases [20]. Optimally-sized multi-element receiver array coils can also reduce image distortion using accelerated parallel imaging techniques, such as GeneRalized Autocalibrating Partially Parallel Acquisitions (GRAPPA) [21] and SENSitivity Encoding (SENSE) [22]. High SNR and reduced distortion are critical in fMRI research at high spatial resolutions [23], motivating continued development of high-density, multi-element coil arrays designed for fMRI of specific brain regions [24]. For example, fMRI using a high-density surface coil array at 7T could detect blood oxygenation level-dependent (BOLD) signal changes at high spatial resolution and acquisition rates when observing human cortical structures [13], [24].

Many previous studies in ultra-high-field MRI used separate transmit-only and receive-only (TORO) coil arrays because the requirements for the Tx coils (efficiency and uniformity) and Rx coils (high SNR, parallel imaging) are different. Typically, the receiver coils are placed as close as possible to the body, while the transmit RF coils are located at a distance from the receiver coils for more homogeneous excitation in the region of interest (ROI). A TORO coil optimized for the occipital region has previously been used for visual cortex functional imaging [13], [24]. Here, the receive coil array was made of small loop coils with high SNR near the skull in the visual cortex region, while a 4-channel phased-array transmit coil was used for homogeneous $B_1^+$ field in the visual cortex. However, without any coil element on the front of the head, there was little signal from the frontal brain to help align the functional images with an anatomical template. In cortical fMRI studies, such alignment is important for the ROI segmentation in data analysis and is required in many standard post-processing pipelines. The lack of a whole-brain signal often necessitates a separate scan with a different (whole brain) coil, adding a burden to the scan workflow. In this study, we propose a new customized 7T visual cortex RF coil that combines a TORO coil array with transmit-and-receive (TRx) coil elements to achieve (i) high SNR in the visual cortex, (ii) availability of whole-brain edge images, and (iii) structural openness in the front for easy delivery of visual stimuli to the participants. We compared the SNR and temporal SNR (tSNR) of four RF coils for 7T human MRI, including a commercial 1Tx/32Rx TORO coil, a custom 6Tx/16Rx TORO coil, a 6TRx array coil, and the proposed RF coil that grafted a 2TRx coil to a 4Tx/14Rx TORO coil (numbers before Tx, Rx, and TRx indicate channel counts) to demonstrate the advantages and potential of the proposed coil. The experimental data showed that the proposed RF coil achieved a higher tSNR than that of the commercial coil in the visual cortex, while maintaining sufficient signal from the anterior brain for the segmentation-based fMRI analysis.

## II. MATERIALS AND METHODS

### A. COIL DESIGN

The visual cortex coil, consisting of three modular parts of (i) the inner module supporting 14 receive-only coil elements, (ii) the outer module supporting four transmit-only and two TRx elements, and (iii) an electronics box in the back, was constructed on an acrylic housing designed to fit the size of a typical adult human head, as shown in Fig. 1. The size and position of the receive-only coil elements were determined to ensure a high SNR in the visual cortex, as shown in Fig. 1b. First, 16 octagonal elements (width = 47 mm) were laid out in a 4 × 4 matrix covering an area of 125 mm × 150 mm (left-right × superior-inferior). Overlap decoupling was used to minimize the mutual inductance between adjacent elements [19]. Subsequently, the initial design was modified by disconnecting two of the 16 elements on the most inferior side, and their corresponding receive chain cables were used for the 2-channel TRx coil (Fig. 1a-b). The outer module was made of a cylindrical shell (outer diameter = 350 mm) with a frontal opening to facilitate visual stimulation (Fig. 1a). Both transmit-only and TRx coils were constructed using a copper tape with a width of 6 mm. All six coil elements had the same rectangular shape with a dimension of 100 mm × 220 mm (side × length) and were arranged angularly at 45° increments without overlap to cover a 270° span. Capacitive decoupling [25] with high-voltage capacitors (Voltronics, Salisbury, MD, USA) reduced coupling between neighboring elements of the transmit array. For comparison, we also operated the coil in the TORO mode using the full (initially designed) 4 × 4 receive coils for signal reception, while utilizing all six elements on the outer housing for RF transmission only. Furthermore, experiments employing the six rectangular elements on the outer housing converted to TRx coils were performed to provide reference for full brain

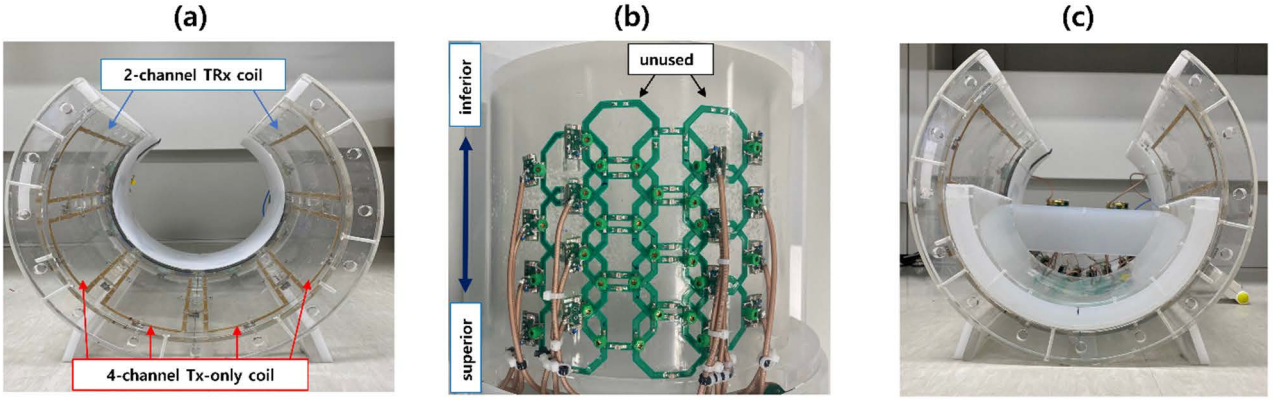


**FIGURE 1.** Custom RF coil for MRI of the visual cortex at 7 Tesla. (a) 6-channel phased array transmit coil including 2-channel TRx (blue arrows) and 4-channel Tx-only (red arrows) coils. (b) 4 × 4 Rx-only coil layout, where 2 channels on the inferior side (near the cerebellum, black arrows) were open and unused. (c) The combined coil with an open structure that facilitates visual stimulation by providing a wide viewing angle.

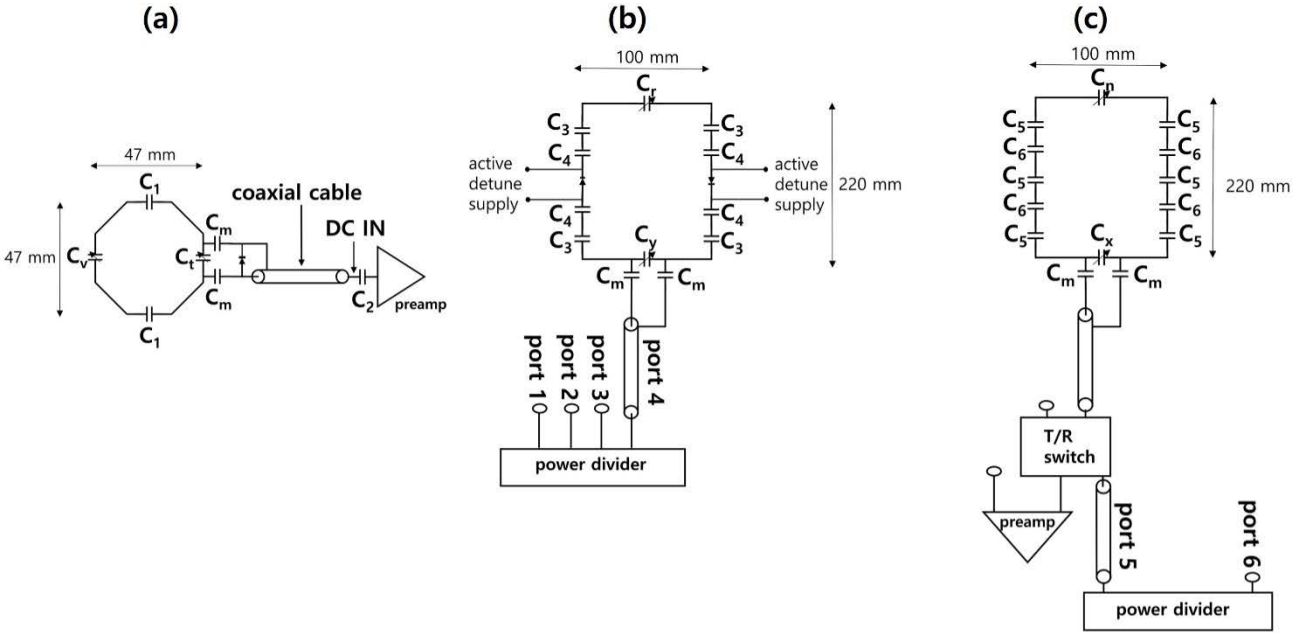


**FIGURE 2.** (a) Schematic diagram of an octagonal receive-only surface loop coil with a width of 47 mm, including a preamplifier and an active detuning circuit. (b) Schematic diagram of a transmit-only surface loop coil including a power divider and an active detuning (diode enable) circuit. (c) Schematic diagram of a transmit/receive surface loop coil including a preamplifier, a T/R switch, and a power divider. All coils were tuned to $^1$H at 7T (300 MHz). Capacitor values: $C_1 = 8.2$ pF, $C_2 = C_m = 470$ pF, $C_3 = 3.6$ pF, $C_4 = 4.7$ pF, $C_5 = 6.2$ pF, $C_6 = 10$ pF, while the variable capacitors $C_V$, $C_n$, $C_t$, $C_x$, $C_r$, $C_y$ could be adjusted within the range of 1 – 23 pF.

coverage. In the following sections, ''TORO coil'' refers to the coil with the 16Rx-only/6Tx-only configuration, ''TRx coil'' refers to the coil with the 6TRx configuration, and ''hybrid coil'' refers to the proposed coil with the 14Rx-4Tx-2TRx configuration. We compared the proposed coil with a commercial 1Tx/32Rx head coil (Nova Medical, Wilmington, MA, USA), to be called the ''Nova coil.''

### B. COIL CIRCUITRY AND BENCH MEASUREMENTS

Fig. 2 shows the circuit diagram of each coil type (Rx only, Tx only, and TRx). All elements were tuned and matched while loaded with a human head in a bench test using a network analyzer (E5063A, Keysight, Santa Rosa, CA, USA). Fig. 2a shows the circuit of one of the 14 received-only coils. Each coil was a regular octagon with a width of 47 mm. Resonant frequency tuning at 300 MHz and impedance matching to 50 Ω were achieved through non-magnetic fixed capacitors with values of $C_1 = 8.2$ pF and $C_m = 470$ pF (Dalian Dalicap Technology, Liaoning, China) and variable capacitors with values of $C_V$ and $C_t = 1 - 23$ pF (Murata Manufacturing, Kyoto, Japan). A DC voltage was applied to the PIN diode to detune the coil during transmission.

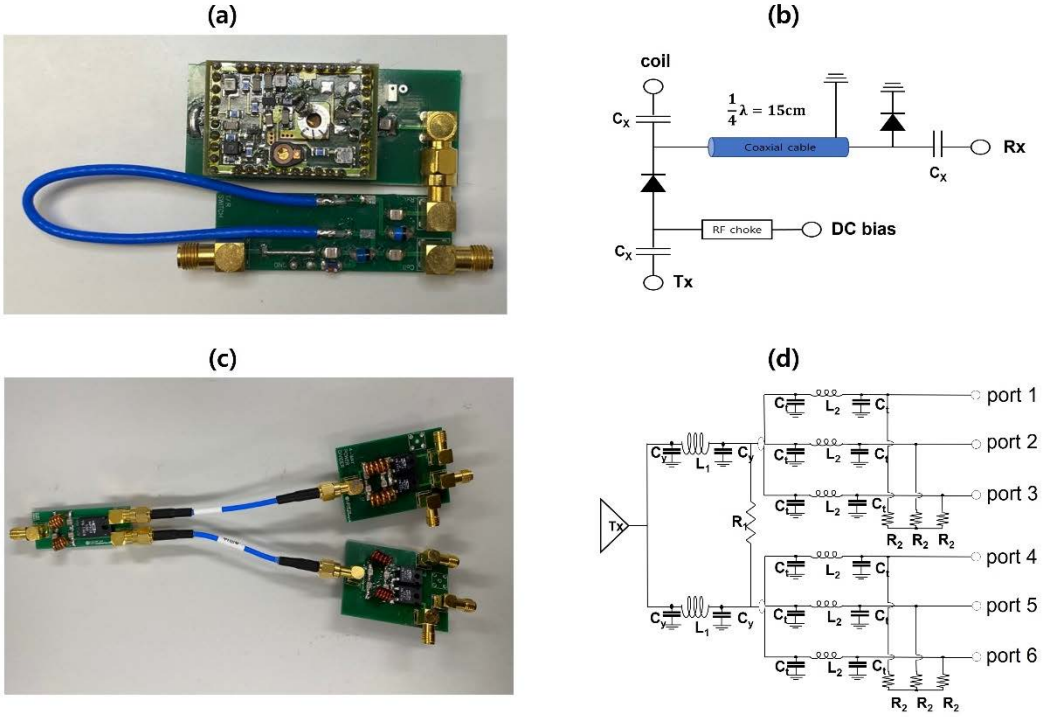


**FIGURE 3.** (a) Picture of the preamplifier and T/R switching circuit. (b) Schematic diagram of the T/R switching circuit. (c-d) 6-way Wilkinson power divider, picture and schematic. Capacitor values: $C_x = 470$ pF, $C_y = 5.6$ pF, $C_t = 2.7$ pF. Inductor values: $L_1 = 39$ nH, $L_2 = 45$ nH. Resistor values: $R_1 = 100\ \Omega$, $R_2 = 50\ \Omega$.

A DC voltage was also used in the preamp circuit board for active detuning. In addition to the overlap decoupling to minimize the mutual inductance of adjacent coils, preamplifier decoupling further reduced coupling among non-adjacent coils. For this, a λ/4 (170 mm) coaxial cable (K02252D, Huber-Suhner, Herisau, Switzerland) connected each coil to a low input-impedance preamplifier (WMA7TRA, WanTcom Inc., Chanhassen, MN, USA) [26]. The decoupling between receive coils was confirmed by S21 measurement using a network analyzer and a dual pickup probe with an isolation of −60 dB. All the preamplifiers were aligned in the z-direction of the 7T scanner to avoid Hall effect problems with field-effect transistors [27]. The tuning and matching of the transmit coil elements shown in Fig. 2b-c were carried out in the same manner as the receive coils. High-power diodes were installed for active detuning for both the transmit-only coil loop and T/R switchboard. The transmit coil elements were enabled when a DC voltage was supplied to the diode. Non-magnetic RG 316 coaxial cables with different phase lengths connected to the coil (Fig. 2b) and between the T/R switch and the power divider (Fig. 2c) were used as phase shifters for circular polarization of the transmitted RF field. The phase difference between the adjacent transmit elements was 45° as confirmed by the network analyzer.

A T/R switch circuit shown in Fig. 3a-b allowed switching between the reception and transmission for the TRx coil elements. When a DC bias was applied to the T/R switchboard, the diode allowed RF transmission to reach the coil element. On the other hand, the coil operated as a receive coil when the DC bias was off. The transmission coefficient (S21) of each T/R switch was measured by a network analyzer. We confirmed that S21 between the coil and Rx was less than −20 dB in the transmit operation and less than −21 dB between the coil and Tx in the receive operation. The power divider consisted of one 2-way and two 3-way Wilkinson dividers (Fig. 3c) [28] with an even distribution of 7 dB power to the six output ports (Fig. 3d), four connected to the Tx-only elements, and two connected to the TRx elements.

### C. SAR SIMULATION

The 6-channel Tx coil array was modeled using perfect electric conductor (PEC) in Sim4Life (Zurich med tech, https://zmt.swiss/sim4life/) to validate the SAR. A single Tx element had a dimension of 100 mm × 220 mm and six elements were placed around a 350 mm diameter cylinder with 10 mm distance between neighboring elements. Each Tx element had 12 distributed capacitors of 6.5 pF each and a single input-voltage source. The input signal was set to a gaussian pulse (center frequency: 300 MHz, bandwidth: 600 MHz). The 6Tx coil array was positioned around the brain region of a human body model, the Duke model (ITIS Foundation, Zurich, https://itis.swiss/). The input power to the coil ports was adjusted so that the magnitude of B1+ at the center of the brain was 2 uT [29], and 10g-averaged SAR was measured.

### D. MRI SCAN

All experiments were performed using a 7T whole-body MRI scanner (Magnetom Terra, Siemens Healthineers, Erlangen, Germany). The MRI scans were obtained from two healthy male volunteers (ages 30 and 20) who submitted an informed consent following protocols approved by the Institutional Review Board of Sungkyunkwan University. Table 1 lists the scan parameters for all experiments. The flip angle was experimentally optimized for each coil through manual adjustment of transmission voltage. All scans were acquired on the axial plane with the phase encoding in the left-right direction.

**TABLE 1. Scan parameters for all experiments.**

| | Experiment 1 | Experiment 2 | Experiment 3 | |
|---|---|---|---|---|
| Coils | hybrid coil, Nova coil | hybrid coil, TORO coil, TRx coil | hybrid coil | |
| Sequence parameters | EPI, 0.5 mm in-plane resolution | GRE | T1-weighted (MP2RAGE) | EPI, 1.2mm$^3$ isotropic |
| Number of EPI volumes | 72 | | | 150 |
| Repetition time (ms) | 2500 | 2110 | 4300 | 2000 |
| Echo time (ms) | 27 | 20 | 1.9 | 20 |
| Slice thickness (mm) | 0.8 | 3.5 | 1 | 1.2 |
| Number of slices | 72 | 50 | 144 | 108 |
| Matrix | 152 × 304 | 420× 640 | 238 × 240 | 174 × 174 |
| Voxel size (mm$^3$) | 0.5 × 0.5 × 0.8 | 0.46 × 0.34 × 3.5 | 0.83 × 0.83 × 1 | 1.2 × 1.2 × 1.2 |
| Acquisition type | 2D | 2D | 3D | 2D |
| Bandwidth (Hz/pixel) | 820 | 60 | 250 | 1690 |
| Averages | 1 | 1 | 1 | 1 |
| Acceleration factor | 6 | 3 | 3 | 9 |
| Reference lines PE | 54 | 48 | 32 | 84 |
| Phase partial Fourier | 6/8 | 6/8 | 6/8 | 6/8 |
| Field of view (mm$^2$) | 76 × 152 | 192 × 220 | 198 × 199 | 209 × 209 |
| Scan time (s) | 180 | 286 | 340 | 300 |

In the first experiment, the tSNR of the visual stimulation fMRI was compared between the hybrid coil and the Nova coil. Volunteer 1 (age = 30) was scanned using an echo-planar imaging (EPI) sequence with an in-plane resolution of 0.5 mm and volume repetition time of 2.5 s. During the scan, the volunteer observed ''drifting grating'' visual stimuli delivered from a projector through a mirror. The grating drifted at a velocity of 4 periods/sec and its direction was reversed every second. The orientation of the grating cycled through 0, 45, 90 and 135°, changing every 10 seconds. A total of 8.5 cycles per run were completed, and one run was collected for each coil. The second experiment compared the anatomical coverage and SNR performance of the hybrid coil, TORO coil and the TRx coil. Here, volunteer 2 (age = 20) was scanned with a fast spoiled gradient echo (GRE, vendor name: FLASH) sequence in the axial plane with very high in-plane resolution (0.1 mm). In the third experiment, volunteer 2 was scanned with a longitudinal relaxation time (T1)-weighted anatomical imaging sequence (MP2RAGE) and an EPI sequence for visual stimulation fMRI in the hybrid coil. During the EPI scan, the volunteer performed a visual field mapping task (population receptive field estimation) [30], [31]. In the task, a bar-shaped aperture slowly swept (at 28 sec/cycle) over a circle-shaped cartoon image in the background, which changed at 7.5 Hz. Four bar aperture orientations and two opposite motion directions for each bar were used within a cycle. A total of 8 cycles were completed within a run and 3 runs were collected from the volunteer. The volunteer was instructed to fixate on the dot at the center of the screen and to press a button when the dot changed color. The EPI time series and the anatomical images were processed for standard visual field mapping analysis, as explained in the next section.

### E. $B_1^+$ MAPPING SCANS

For the flip angle measurement of the Nova coil and the hybrid coil, the Double Angle Method (DAM) was utilized [32] with $\alpha_1$ and $\alpha_2$ set as 40° and 80°, respectively. We scanned two spherical phantoms: a vendor-provided liquid spherical phantom (Model spherical D165, Blue), containing an aqueous solution of 8.2 g/L NaC2H3O2, 9.6 g/L C3H5O3Li, and a spherical oil phantom (Model spherical D165, SPECTR.1H), containing oil of 0.011 g/L MACROLEX blue. The flip angle data were quantitatively compared through 1D profiling in the posterior part to the phantom corresponding to the occipital lobe of the human brain.

### F. fMRI DATA ANALYSIS

To measure tSNR in Experiment 1, the EPI time series from each voxel was linearly detrended, high-pass filtered (0.0001 Hz, 2nd order IIR filter), and scaled to its average intensity value. Subsequently, tSNR was computed as the temporal mean of the scaled time series divided by the temporal standard deviation. For comparison between the hybrid coil and the Nova coil, the tSNR was averaged over the voxels across the medial-lateral axis after excluding the non-brain voxels, yielding an average tSNR value for each location along the anterior-posterior axis.

To visualize functional activation maps on the cortical surface, functional volume data need to be projected to a reconstructed cortical surface. Since standard software for volume-to-surface projection, such as FreeSurfer and AFNI, takes whole-brain anatomical images as input, anatomical images that do not cover the whole-brain are difficult to use for this purpose. As a critical test of the utility of the proposed

hybrid coil, we investigated the possibility of surface projection with partially low-SNR anatomical images acquired from the coil, using the data collected in Experiment 3. For this, we first estimated from the EPI time series data, the position of the population receptive field of each voxel was estimated using BOLD responses during the task with a compressive spatial summation (CSS) model [31]. The results of the visual field mapping analysis were then projected onto the cortical surface as follows: 1) The anatomical images were corrected using ANTs for intensity uniformity [33], and the skull was removed using FSL [34]. 2) The anatomical images were segmented using FreeSurfer [35] into the gray matter (GM), white matter (WM), and cerebrospinal fluid (CSF). The inflated surface of the cerebral cortex was reconstructed based on the boundary between GM and WM. 3) Functional images were also corrected for intensity uniformity with AFNI [36] and skull-stripped with FSL to register functional results to the surface. 4) Lastly, registration between the surface and functional images was performed using AFNI.

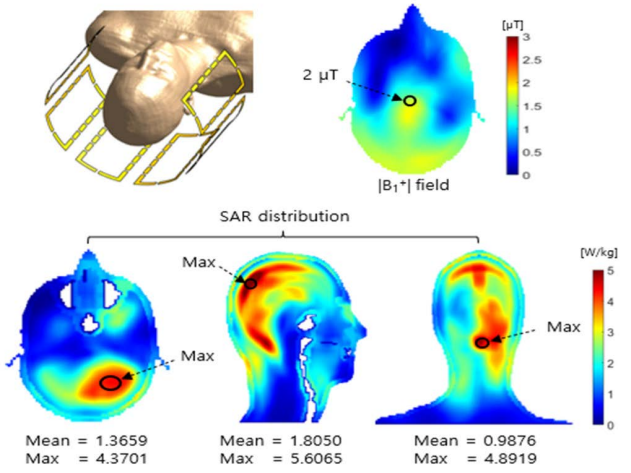


**FIGURE 4.** $B_1^+$ field and 10g averaged SAR distribution in the human head model with the maximum and mean SAR values indicated.

## III. RESULTS

Table 2a shows that each receive element of the 14-channel receive-only and 2-channel TRx coils was impedance-matched to less than −24 dB in S11; coupling (S21) between adjacent receive-only elements was found to be less than −13 dB. The receive-only array is small in size, and far from the 2-channel TRx coil, so the S21 between the receive-only coil and TRx coil elements were measured to be less than −30 dB. Table 2b shows that each transmit element of the 4-channel transmit-only and 2-channel TRx coils had S11 lower than −22 dB. The S21 between adjacent transmitting elements was less than −14 dB.

Fig. 4 shows the result of the SAR simulation. the input power at each port was 27 W. The mean value over the whole brain and the local maximum of 10g-averaged SAR were 1.5173 W/kg and 5.6393 W/kg, respectively This compares with the average and maximum SAR values of a typical head birdcage coil at 300MHz of 1.45 W/kg and 6.72 W/kg [29].

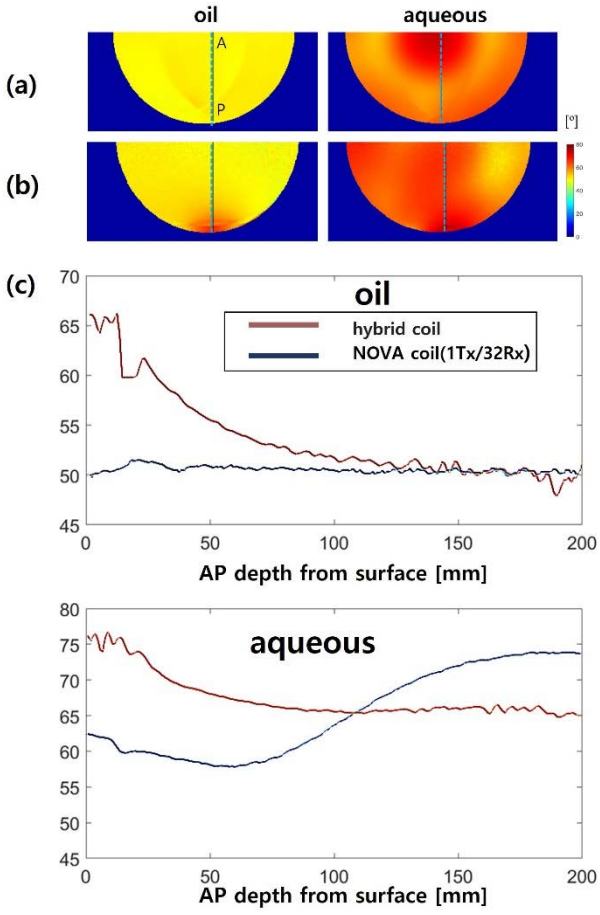


**FIGURE 5.** Flip angle maps (in degrees) obtained using two spherical phantoms (oil and aqueous) for comparison of flip angle homogeneity in NOVA coil (a) and hybrid coil (b). 1D profiles of the flip angles along the vertical lines in (a,b) are compared in (c).

Fig. 5 compares flip angel maps obtained from the two phantoms. The Nova coil showed relatively uniform flip angles in the oil phantom. However, the hybrid coil showed higher transmission efficiency near the phantom's edge in the occipital region. In the aqueous phantom, the Nova coil showed high transmission efficiency mainly at the center of the sphere, and significantly lower efficiency near the bottom which corresponds to the visual cortex. On the other hand, the hybrid coil showed higher transmission efficiency in the periphery and overall better $B_1^+$ homogeneity across the aqueous phantom.

Fig. 6a-b shows 0.5 mm in-plane resolution EPI images near the visual cortex obtained using the hybrid coil and the NOVA coil. Both images have the same color scale, showing that the hybrid coil has much higher SNR in the visual cortex near the skull. For quantitative comparison, the slices in the

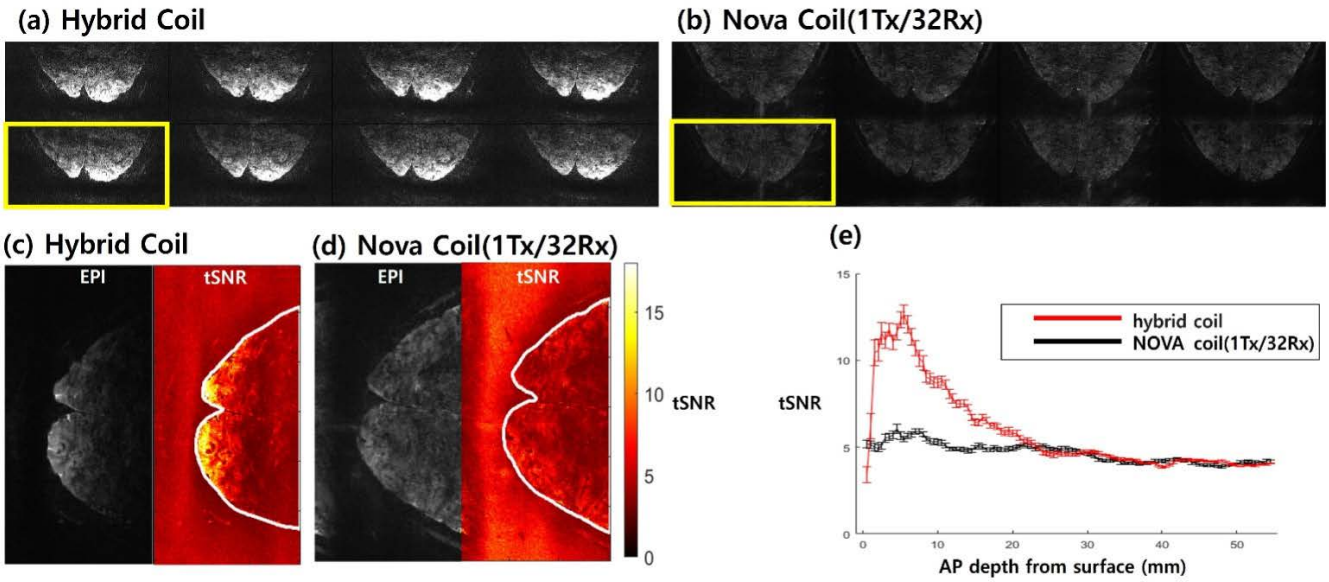


**FIGURE 6.** (a,b) Axial 2D EPI images obtained from the hybrid coil (a) and the NOVA coil (b). (c,d) Comparison of tSNR in the visual cortex between the hybrid coil (c) and the NOVA coil (d). Plots of the average tSNR along the AP axis are shown in (e), where the x-axis represents the distance from the posterior end of the brain.

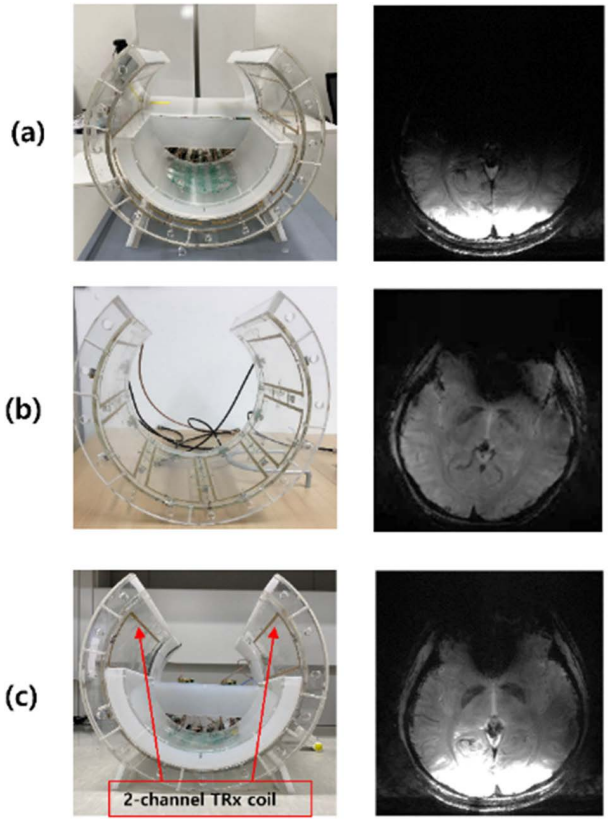


**FIGURE 7.** Pictures of the custom-built coils and example images produced by them. (a) 6Tx/16Rx TORO coil. (b) 6-channel TRx coil. (c) 2TRx coil grafted to a 4Tx/14Rx coil (hybrid coil). The images on the right are on the same grayscale.

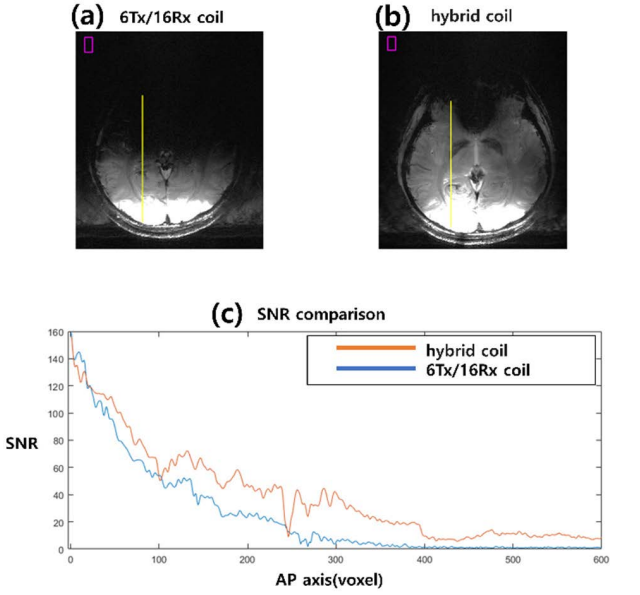


**FIGURE 8.** SNR comparison between the images obtained with the 6Tx/16Rx TORO coil (a) and the hybrid coil (b). The SNR profiles in (c) were obtained from the image intensities along the yellow lines divided by the noise calculated in the purple box of the respective images.

yellow boxes in Fig. 6a-b were analyzed for tSNR as shown in Fig. 6c-e. The 1D tSNR profiles in Fig. 6(e) were calculated along the AP axis excluding the skull. It can be seen that the hybrid coil has about 2.5 times higher tSNR than the commercial (Nova) coil in the visual cortex region close to the receiving coil.

Fig. 7 shows the axial GRE images obtained from Volunteer 2 using the three custom-built coils (TORO, TRx, and hybrid coils). Fig. 7a shows that the 6Tx/16Rx TORO coil achieved a very high SNR in the visual cortex area, but the SNR quickly diminished in the anterior region. In contrast, the 6-channel TRx coil shown in Fig. 7b is capable of

**TABLE 2.** S-parameter matrices of the hybrid coil.

(a) S-parameters of the receive coil.

| Channel | 1Rx | 2Rx | 3Rx | 4Rx | 5Rx | 6Rx | 7Rx | 8Rx | 9Rx | 10Rx | 11Rx | 12Rx | 13Rx | 14Rx | 1Tx/Rx | 2Tx/Rx |
|---|---|---|---|---|---|---|---|---|---|---|---|---|---|---|---|---|
| 1Rx | -25.5 | -24.3 | -15.2 | -15.2 | -17.6 | -14.6 | -14.2 | -23.6 | -14.3 | -18.6 | -25.6 | -25.3 | -28.3 | -24.3 | -30.2 | -33.2 |
| 2Rx | | -24.3 | -14.1 | -15.5 | -14.3 | -13.6 | -13.4 | -18.3 | -14.5 | -16.2 | -24.6 | -28.6 | -27.6 | -28.5 | -31.6 | -35.1 |
| 3Rx | | | -27.1 | -17.5 | -13.9 | -20.2 | -17.6 | -15.2 | -13.3 | -18.6 | -15.5 | -19.1 | -24.3 | -25.2 | -32.3 | -32.3 |
| 4Rx | | | | -25.5 | -15.7 | -14.3 | -13.6 | -13.5 | -13.2 | -15.5 | -19.1 | -24.3 | -25.2 | -20.9 | -35.2 | -34.0 |
| 5Rx | | | | | -25.5 | -16.8 | -15.8 | -14.7 | -15.2 | -15.3 | -15.4 | -19.2 | -17.3 | -15.2 | -35.3 | -30.2 |
| 6Rx | | | | | | -25.2 | -15.7 | -13.6 | -16.6 | -13.6 | -16.6 | -17.4 | -19.4 | -15.8 | -32.1 | -31.2 |
| 7Rx | | | | | | | -24.0 | -13.5 | -14.3 | -16.3 | -14.3 | -17.4 | -19.4 | -15.8 | -36.2 | -34.2 |
| 8Rx | | | | | | | | -25.3 | -17.3 | -18.2 | -15.3 | -19.3 | -18.1 | -14.3 | -35.1 | -34.5 |
| 9Rx | | | | | | | | | -28.1 | -14.8 | -15.8 | -17.2 | -17.2 | -14.2 | -32.2 | -30.2 |
| 10Rx | | | | | | | | | | -25.1 | -14.3 | -14.2 | -14.2 | -15.3 | -30.2 | -35.3 |
| 11Rx | | | | | | | | | | | -25.6 | -13.6 | -15.3 | -14.6 | -30.4 | -31.5 |
| 12Rx | | | | | | | | | | | | -25.2 | -13.2 | -15.2 | -33.5 | -36.3 |
| 13Rx | | | | | | | | | | | | | -24.3 | -14.9 | -36.3 | -31.3 |
| 14Rx | | | | | | | | | | | | | | -26.3 | -34.2 | -32.5 |
| 1Tx/Rx | | | | | | | | | | | | | | | -23.2 | -35.2 |
| 2Tx/Rx | | | | | | | | | | | | | | | | -24.3 |


(b) S-parameters of the transmit coil.

| Channel | 1Tx/Rx | 1Tx | 2Tx | 3Tx | 4Tx | 2Tx/Rx |
|---|---|---|---|---|---|---|
| 1Tx/Rx | -22.2 | -14.3 | -15.3 | -15.2 | -16.5 | -17.2 |
| 1Tx | | -24.3 | -14.1 | -14.3 | -15.2 | -15.3 |
| 2Tx | | | -25.3 | -16.1 | -13.9 | -14.3 |
| 3Tx | | | | -25.3 | -14.3 | -15.3 |
| 4Tx | | | | | -24.5 | -16.2 |
| 2Tx/Rx | | | | | | -23.2 |


producing a relatively uniform whole-brain image despite low SNR. On the other hand, Fig. 7c shows that the proposed hybrid coil successfully produced a whole-brain image and achieved high SNR in the visual cortex. The increased visibility of the frontal brain compared to the TORO configuration shown in Fig. 7a is due to the presence of two receiving elements of the 2TRx coil (red arrows in Fig. 7c). This can help align the functional images in the visual cortex with the whole-brain anatomical template. Fig. 8 presents the SNR of the images obtained from the TORO coil and the hybrid coil along a line in the AP direction. The two coils exhibit similar SNR levels in the visual cortex region, indicating that the omission of two receive-only elements (i.e., going from 16 to 14Rx) in the hybrid coil configuration cost little signal in the region.

On the other hand, the advantage of the hybrid coil is manifest in the middle and anterior brain, where the TORO coil quickly loses signal sensitivity and SNR.

Fig. 9 shows the results of the cortical surface reconstruction. Although part of the left frontal area showed poor image quality (Fig. 9a, the area filled in light gray), the skull was removed properly (Fig. 9b) based on the whole-brain image. The segmentation (Fig. 9c) and the cortical surface reconstruction (Fig. 9d) appeared reasonable, except in the left frontal area. The software incorrectly segmented the corresponding area because of the insufficient signal in the frontal region. Since the main purpose of the hybrid coil was to image the visual cortex at high resolution and capture the whole-brain edges, such localized segmentation error was not critical in itself. To confirm the quality of the overall segmentation and the reconstruction of the visual cortex, the results of the visual field mapping analysis were projected onto the reconstructed surface (Fig. 10). We found projected visual field maps closely matched previously reported results in the literature [29]: the polar angle map (Fig. 10a) as distinct stripes representing the mirror-symmetric spatial layout of the early and intermediate visual areas, including V1, V2, and V3, and the eccentricity map (Fig. 10b) as concentric circles spanning from the foveal representation close to the occipital pole on the lateral surface to increasingly peripheral representations at more anterior portions of the occipital cortex along the medial surface. These results validate the segmentation and cortical surface reconstruction applied to the visual cortex data from the hybrid coil.

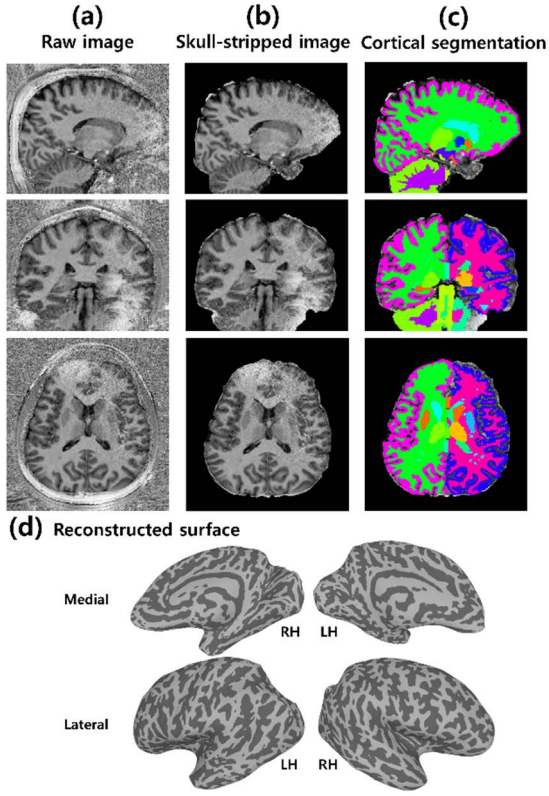


**FIGURE 9.** Surface reconstruction of anatomical images acquired with the hybrid coil. (a) Raw anatomical images before skull-stripping. (b) Skull stripped images. (c) Cortical segmentation. (d) Reconstructed surfaces.

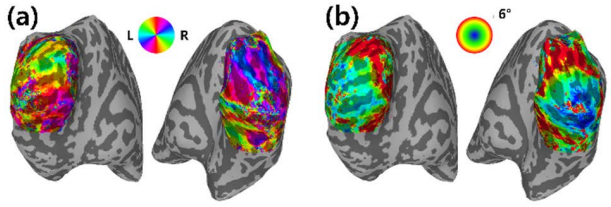


**FIGURE 10.** The results of the visual field mapping analysis projected onto the reconstructed cortical surfaces. (a) Polar angle map. (b) Eccentricity map.

## IV. DISCUSSION AND CONCLUSION

Several studies in the literature reported SNR improvements in ultra-high-field human neuroimaging using region-specific Rx-only coil and TRx coil combination [37]–[39]. However, these coils were not specifically designed for visual stimulation studies, as they had a closed structure with a transmit coil surrounding the head which can be in the way for stimulation delivery. On the other hand, most RF coils that specifically targeted the visual cortex did not allow imaging of the frontal brain due to the lack of receiving elements in the front [13], [24]. In this study, we achieved high SNR in the visual cortex while accommodating the need for whole-brain coverage for post-processing using a hybrid RF coil. This was accomplished by utilizing 2 TRx elements that were strategically placed on the front of the coil to preserve its open structure. In our coil, RF transmission was executed by six rectangular transmitter elements installed on the outer layer of the cylindrical coil housing. Out of the six elements, four were arranged to cover the posterior half of the housing and were configured as transmit-only. The other two elements on the frontal side functioned as both Tx and Rx coils to minimize the RF components in the front for maximal openness. A high SNR in visual cortex imaging was achieved by high-density arrangement of 14 receive-only elements on the inner layer of the housing near the area where the participant's head contacted the coil. The hybrid coil enabled high-resolution anatomical and functional image acquisition of the visual cortex at 7T (Fig. 6) and produced whole-brain edge images to facilitate data analysis, as shown in Figs. 8 and 9.

The low coupling among the TRx coils, transmit-only coils, and receive-only coils was verified through the bench test. The coupling between the TRx coil elements and the transmit-only coil elements was minimized by capacitive decoupling to ensure that the S21 parameter was less than $-13$ dB. The coupling between the receive-only elements and the TRx elements was low (S21 $< -30$ dB) due to the large distance ($\sim$200 mm) between them. The 14 channel Rx-only array of the proposed hybrid coil was made of relatively small loop coils with a diameter of approximately 47 mm. These coil elements have optimal imaging depths of approximately 50 mm at 7T [20], which is adequate for visual cortex imaging with high SNR, as confirmed in our study. The Nova coil (1Tx/32Rx) and the hybrid coil were compared in terms of image quality in high resolution (0.5 mm in-plane) EPI in the axial plane. It was confirmed that the hybrid coil had approximately 2.5 times higher tSNR than the Nova coil in the visual cortex close to the receiving coils.

The SNR in the frontal part of the brain is currently marginal for the hybrid coil. However, this can potentially be increased by placing more receive elements in the front part of the coil without compromising the openness of the structure. This will allow for more robust whole-brain imaging for patients with different head shapes and sizes.

In our experiments, the RF transmission was approximately in the CP mode, with different Tx elements transmitting at geometrically fixed phase delays. The SAR simulation (Fig. 4) indicated that the 10g-averaged SAR of the proposed coil was comparable to or lower than the corresponding values for a typical birdcage coil. Furthermore, our $B_n1^+$ efficiency and homogeneity (Fig. 5) were relatively high compared to the commercial coil especially for an aqueous phantom, which better mimics a human head than oil. In particular, the center brightening effect of conventional birdcage coils or TEM head coils [3] was greatly reduced due to the high transmission efficiency in the peripheral region of the brain.

Although we obtained acceptable whole-brain images for functional image analysis, the RF homogeneity and image quality can be further increased by adopting RF shimming and pTx strategies [8] within the existing transmit coil

hardware and system capability. This will be investigated in future studies.

In conclusion, we presented a hybrid RF coil specially configured for visual stimulation studies in 7T MRI. We proposed a novel RF coil structure, which combines a TORO coil and a TRx coil, to achieve high signal sensitivity and resolution in the visual cortex while allowing whole-brain edge imaging for functional analysis based on the standard software. Our coil is expected to find use in high-quality visual stimulation studies in ultra-high-field MRI.

## REFERENCES

[1] M. B. Hoffmann, J. Stadler, M. Kanowski, and O. Speck, "Retinotopic mapping of the human visual cortex at a magnetic field strength of 7 T," *Clin. Neurophysiol.*, vol. 120, no. 1, pp. 108–116, Jan. 2009.

[2] C. A. Olman, P.-F. Van de Moortele, J. F. Schumacher, J. R. Guy, K. Uğurbil, and E. Yacoub, "Retinotopic mapping with spin echo BOLD at 7 T," *Magn. Reson. Imag.*, vol. 28, no. 9, pp. 1258–1269, Nov. 2010.

[3] J. T. Vaughan, M. Garwood, C. M. Collins, W. Liu, L. DelaBarre, G. Adriany, P. Andersen, H. Merkle, R. Goebel, M. B. Smith, and K. Ugurbil, "7 T vs. 4 T: RF power, homogeneity, and signal-to-noise comparison in head images," *Magn. Reson. Med., Off. J. Int. Soc. Magn. Reson. Med.*, vol. 46, no. 1, pp. 24–30, 2001.

[4] P. A. Bottomley and E. R. Andrew, "RF magnetic field penetration, phase shift and power dissipation in biological tissue: Implications for NMR imaging," *Phys. Med. Biol.*, vol. 23, no. 4, p. 630, 1978.

[5] P. Röschmann, "Radiofrequency penetration and absorption in the human body: Limitations to high-field whole-body nuclear magnetic resonance imaging," *Med. Phys.*, vol. 14, no. 6, pp. 922–931, Nov. 1987.

[6] Z. Cao, X. Yan, J. C. Gore, and W. A. Grissom, "Designing parallel transmit head coil arrays based on radiofrequency pulse performance," *Magn. Reson. Med.*, vol. 83, no. 6, pp. 2331–2342, Jun. 2020.

[7] Z. Cao, X. Yan, and W. A. Grissom, "Array-compressed parallel transmit pulse design," *Magn. Reson. Med.*, vol. 76, no. 4, pp. 1158–1169, Oct. 2016.

[8] S.-K. Lee, S. Oh, H.-S. Kim, and B.-P. Song, "Radio-frequency vector magnetic field mapping in magnetic resonance imaging," *IEEE Trans. Med. Imag.*, vol. 40, no. 3, pp. 963–973, Mar. 2021.

[9] G. R. Morrell and M. C. Schabel, "An analysis of the accuracy of magnetic resonance flip angle measurement methods," *Phys. Med. Biol.*, vol. 55, no. 20, p. 6157, 2010.

[10] P.-F. Van de Moortele, C. Akgun, G. Adriany, S. Moeller, J. Ritter, C. M. Collins, M. B. Smith, J. T. Vaughan, and K. Uğurbil, "$B_1$ destructive interferences and spatial phase patterns at 7 T with a head transceiver array coil," *Magn. Reson. Med.*, vol. 54, no. 6, pp. 1503–1518, 2005.

[11] G. C. Wiggins, A. Potthast, C. Triantafyllou, C. J. Wiggins, and L. L. Wald, "Eight-channel phased array coil and detunable TEM volume coil for 7 T brain imaging," *Magn. Reson. Med., Off. J. Int. Soc. Magn. Reson. Med.*, vol. 54, no. 1, pp. 235–240, 2005.

[12] G. Adriany, "Transmit and receive transmission line arrays for 7 Tesla parallel imaging," *Magn. Reson. Med., Off. J. Int. Soc. Magn. Reson. Med.*, vol. 53, no. 2, pp. 434–445, Feb. 2005.

[13] S. Sengupta, A. Roebroeck, V. G. Kemper, B. A. Poser, J. Zimmermann, R. Goebel, and G. Adriany, "A specialized multi-transmit head coil for high resolution fMRI of the human visual cortex at 7 T," *PLoS ONE*, vol. 11, no. 12, Dec. 2016, Art. no. e0165418.

[14] R. Lattanzi and D. K. Sodickson, "Ideal current patterns yielding optimal signal-to-noise ratio and specific absorption rate in magnetic resonance imaging: Computational methods and physical insights," *Magn. Reson. Med.*, vol. 68, no. 1, pp. 286–304, Jul. 2012.

[15] G. C. Wiggins, C. Triantafyllou, A. Potthast, A. Reykowski, M. Nittka, and L. L. Wald, "32-channel 3 Tesla receive-only phased-array head coil with soccer-ball element geometry," *Magn. Reson. Med., Off. J. Int. Soc. Magn. Reson. Med.*, vol. 56, no. 1, pp. 216–223, 2006.

[16] G. C. Wiggins, J. R. Polimeni, A. Potthast, M. Schmitt, V. Alagappan, and L. L. Wald, "96-channel receive-only head coil for 3 Tesla: Design optimization and evaluation," *Magn. Reson. Med., Off. J. Int. Soc. Magn. Reson. Med.*, vol. 62, no. 3, pp. 754–762, Sep. 2009.

[17] T. Jaermann, N. De Zanche, P. Staempfli, K. P. Pruessmann, A. Valavanis, P. Boesiger, and S. S. Kollias, "Preliminary experience with visualization of intracortical fibers by focused high-resolution diffusion tensor imaging," *Amer. J. Neuroradiol.*, vol. 29, no. 1, pp. 146–150, Jan. 2008.

[18] J. Breslau, R. W. Dalley, J. S. Tsuruda, C. E. Hayes, and K. R. Maravilla, "Phased-array surface coil MR of the orbits and optic nerves," *Amer. J. Neuroradiol.*, vol. 16, no. 6, pp. 1247–1251, 1995.

[19] P. B. Roemer, W. A. Edelstein, C. E. Hayes, S. P. Souza, and O. M. Mueller, "The NMR phased array," *Magn. Reson. Med.*, vol. 16, no. 2, pp. 192–225, Nov. 1990.

[20] A. Kumar, W. A. Edelstein, and P. A. Bottomley, "Noise figure limits for circular loop MR coils," *Magn. Reson. Med., Off. J. Int. Soc. Magn. Reson. Med.*, vol. 61, no. 5, pp. 1201–1209, May 2009.

[21] M. A. Griswold, P. M. Jakob, R. M. Heidemann, M. Nittka, V. Jellus, J. Wang, B. Kiefer, and A. Haase, "Generalized autocalibrating partially parallel acquisitions (GRAPPA)," *Magn. Reson. Med. Off. J. Int. Soc. Magn. Reson. Med.*, vol. 47, no. 6, pp. 1202–1210, 2002.

[22] K. P. Pruessmann, M. Weiger, M. B. Scheidegger, and P. Boesiger, "SENSE: Sensitivity encoding for fast MRI," *Magn. Reson. Med. Off. J. Int. Soc. Magn. Reson. Med.*, vol. 42, no. 5, pp. 952–962, 1999.

[23] C. Triantafyllou, J. R. Polimeni, and L. L. Wald, "Physiological noise and signal-to-noise ratio in fMRI with multi-channel array coils," *NeuroImage*, vol. 55, no. 2, pp. 597–606, Mar. 2011.

[24] N. Petridou, M. Italiaander, B. L. van de Bank, J. C. W. Siero, P. R. Luijten, and D. W. J. Klomp, "Pushing the limits of high-resolution functional MRI using a simple high-density multi-element coil design," *NMR Biomed.*, vol. 26, no. 1, pp. 65–73, Jan. 2013.

[25] C. von Morze, J. Tropp, S. Banerjee, D. Xu, K. Karpodinis, L. Carvajal, C. P. Hess, P. Mukherjee, S. Majumdar, and D. B. Vigneron, "An eight-channel, nonoverlapping phased array coil with capacitive decoupling for parallel MRI at 3 T," *Concepts Magn. Reson. B, Magn. Reson. Eng.*, vol. 31B, no. 1, pp. 37–43, 2007.

[26] A. Reykowski, S. M. Wright, and J. R. Porter, "Design of matching networks for low noise preamplifiers," *Magn. Reson. Med.*, vol. 33, no. 6, pp. 848–852, 1995.

[27] C. Possanzini and M. Boutelje, "Influence of magnetic field on preamplifiers using GaAs FET technology," in *Proc. 16th Annu. Meeting ISMRM*, 2008, p. 1123.

[28] D. M. Pozar, *Microwave Engineering*. Hoboken, NJ, USA: Wiley, 2011.

[29] C. M. Collins and M. B. Smith, "Signal-to-noise ratio and absorbed power as functions of main magnetic field strength, and definition of '90°' RF pulse for the head in the birdcage coil," *Magn. Reson. Med., Off. J. Int. Soc. Magn. Reson. Med.*, vol. 45, no. 4, pp. 684–691, 2001.

[30] S. O. Dumoulin and B. A. Wandell, "Population receptive field estimates in human visual cortex," *NeuroImage*, vol. 39, no. 2, pp. 647–660, Jan. 2008.

[31] K. N. Kay, J. Winawer, A. Mezer, and B. A. Wandell, "Compressive spatial summation in human visual cortex," *J. Neurophysiol.*, vol. 110, no. 2, pp. 481–494, Jul. 2013.

[32] C. H. Cunningham, J. M. Pauly, and K. S. Nayak, "Saturated double-angle method for rapid $B_1+$ mapping," *Magn. Reson. Med., Off. J. Int. Soc. Magn. Reson. Med.*, vol. 55, no. 6, pp. 1326–1333, 2006.

[33] B. B. Avants, N. J. Tustison, G. Song, P. A. Cook, A. Klein, and J. C. Gee, "A reproducible evaluation of ANTs similarity metric performance in brain image registration," *NeuroImage*, vol. 54, no. 3, pp. 2033–2044, Feb. 2011.

[34] S. Smith, P. R. Bannister, C. Beckmann, M. Brady, S. Clare, D. Flitney, P. Hansen, M. Jenkinson, D. Leibovici, B. Ripley, M. Woolrich, and Y. Zhang, "FSL: New tools for functional and structural brain image analysis," *NeuroImage*, vol. 13, no. 6, p. 249, Jun. 2001.

[35] B. Fischl, M. I. Sereno, and A. M. Dale, "Cortical surface-based analysis: II: Inflation, flattening, and a surface-based coordinate system," *NeuroImage*, vol. 9, no. 2, pp. 195–207, Feb. 1999.

[36] R. W. Cox, "AFNI: Software for analysis and visualization of functional magnetic resonance neuroimages," *Comput. Biomed. Res.*, vol. 29, no. 3, pp. 162–173, Jun. 1996.

[37] N. I. Avdievich, I. A. Giapitzakis, A. Pfrommer, T. Borbath, and A. Henning, "Combination of surface and 'vertical' loop elements improves receive performance of a human head transceiver array at 9.4 T," *NMR Biomed.*, vol. 31, no. 2, p. e3878, Feb. 2018.

[38] K.-N. Kim, P. Heo, Y.-B. Kim, and G.-C. Han, "Magnetic resonance imaging of the inner ear by using a hybrid radiofrequency coil at 7 T," *J. Korean Phys. Soc.*, vol. 66, no. 2, pp. 175–182, Jan. 2015.

[39] V. Pfaffenrot, S. Brunheim, S. H. G. Rietsch, P. J. Koopmans, T. M. Ernst, O. Kraff, S. Orzada, and H. H. Quick, "An 8/15-channel Tx/Rx head neck RF coil combination with region-specific $B_1+$ shimming for whole-brain MRI focused on the cerebellum at 7 T," *Magn. Reson. Med.*, vol. 80, no. 3, pp. 1252–1265, Sep. 2018.

**HYEONG-SEOP KIM** received the B.S. degree in biomedical engineering from Gachon University, Incheon, Republic of Korea, in 2019. He is currently pursuing the integrated M.S. and Doctorate degrees in intelligent precision healthcare convergence with Sungkyunkwan University, Suwon, Republic of Korea.

His research interest includes RF coils called human 7T multi-channel RF coil development for high-resolution visual cortex imaging.

**BYUNG-PAN SONG** received the B.S. degree in biomedical engineering from Gachon University, Incheon, Republic of Korea, in 2019. He is currently pursuing the M.S. degree in global biomedical engineering with Sungkyunkwan University, Suwon, Republic of Korea.

His research interest includes RF coils called histology coil development for micro-tissue MR microscopy.

**ROYOUNG KIM** received the B.S. degree in chemistry and the B.A. degree in psychology from Ewha Womans University, Seoul, South Korea, in 2020. She is currently pursuing the M.S. degree in computational cognitive neuroscience with Sungkyunkwan University, Suwon, South Korea.

Her research interests include cortical layer-dependent human fMRI and feedback connections in the human visual cortex.

**WOO-CHUL CHOI** received the B.S. and M.S. degrees in bio and brain engineering and the Ph.D. degree in brain and cognitive engineering from the Korea Advanced Institute of Science and Technology, South Korea, in 2014, 2016, and 2020, respectively.

Since 2020, he has been working as a Postdoctoral Researcher with the Korea Advanced Institute of Science and Technology. His research interests include human visual perception and imaging human visual cortex using ultra-high field functional magnetic resonance imaging.

Mr. Choi's honors include the Sejong Science Fellowship (National Research Foundation of Korea).

**DONGHYUK KIM** received the M.S. degree in biomedical engineering from Inje University, in 2014. He is currently pursuing the Ph.D. degree with the Department of Health Sciences and Technology, Gachon University. His research interests include RF coil design and electromagnetic simulation.

**WON MOK SHIM** received the B.A. degree in psychology and the M.S. degree in cognitive science from Yonsei University, in 1998 and 2000, respectively, and the Ph.D. degree in experimental/cognitive psychology from Harvard University, in 2005.

From 2005 to 2007, she was a Postdoctoral Researcher with the Department of Psychology, Harvard University, and from 2007 to 2010, she was a Postdoctoral Fellow with the Department of Brain and Cognitive Sciences, MIT. She was an Assistant Professor with the Department of Psychological and Brain Sciences, Dartmouth College, from 2010 to 2016. Since 2016, she has been an Associate Professor with the Department of Biomedical Engineering, Sungkyunkwan University (SKKU). She is the author of three books and more than 20 articles. Her research interests include how the brain represents and processes perceptual and cognitive information from low-level sensory features to high-level contexts and predictions.

**KYOUNG-NAM KIM** received the Ph.D. degree in electrical engineering and information technology from the University of Duisburg-Essen, Germany, in 2011. He has been an Associate Professor with the Department of Biomedical Engineering, Gachon University, Inchon, Republic of Korea, since 2016. He is currently a MRI Committee Member of the Korean Society of Magnetic Resonance in Medicine. His research interests include medical electronic engineering, MRI systems, electromagnetic field analysis, and RF MRI coils.

**SEUNG-KYUN LEE** received the Ph.D. degree in physics from UC Berkeley, CA, USA, in 2005. From 2005 to 2008, he was a Postdoctoral Research Associate with the Physics Department, Princeton University. In 2008, he joined the GE Global Research Center, Niskayuna, NY, USA, to develop high-field MRI technologies, where he is currently a Principal Scientist. From 2016 to 2021, he has worked on the Academic Faculty with the Department of Biomedical Engineering, Sungkyunkwan University, Suwon, South Korea.